# Microfluidic templating of spatially inhomogeneous protein microgels

Xu, Yufan; Jacquat, Raphaël P.B.; Shen, Yi; Vigolo, Daniele; Morse, David; Zhang, Shuyuan; Knowles, Tuomas P.J.

*DOI:*
10.1002/smll.202000432



*Document Version*
Publisher's PDF, also known as Version of record

*Citation for published version (Harvard):*
Xu, Y, Jacquat, RPB, Shen, Y, Vigolo, D, Morse, D, Zhang, S & Knowles, TPJ 2020, 'Microfluidic templating of spatially inhomogeneous protein microgels', *Small*, vol. 16, no. 32, 2000432, pp. 1-9. https://doi.org/10.1002/smll.202000432

NANO · MICRO small
www.small-journal.com

# Microfluidic Templating of Spatially Inhomogeneous Protein Microgels

*Yufan Xu, Raphaël P. B. Jacquat, Yi Shen, Daniele Vigolo, David Morse, Shuyuan Zhang, and Tuomas P. J. Knowles**

**3D scaffolds in the form of hydrogels and microgels have allowed for more native cell-culture systems to be developed relative to flat substrates. Native biological tissues are, however, usually spatially inhomogeneous and anisotropic, but regulating the spatial density of hydrogels at the microscale to mimic this inhomogeneity has been challenging to achieve. Moreover, the development of biocompatible synthesis approaches for protein-based microgels remains challenging, and typical gelation conditions include UV light, extreme pH, extreme temperature, or organic solvents, factors which can compromise the viability of cells. This study addresses these challenges by demonstrating an approach to fabricate protein microgels with controllable radial density through microfluidic mixing and physical and enzymatic crosslinking of gelatin precursor molecules. Microgels with a higher density in their cores and microgels with a higher density in their shells are demonstrated. The microgels have robust stability at 37 °C and different dissolution rates through enzymolysis, which can be further used for gradient scaffolds for 3D cell culture, enabling controlled degradability, and the release of biomolecules. The design principles of the microgels could also be exploited to generate other soft materials for applications ranging from novel protein-only micro reactors to soft robots.**

Y. Xu, R. P. B. Jacquat, Dr. Y. Shen, D. Morse, S. Zhang, Prof. T. P. J. Knowles
Centre for Misfolding Diseases
Department of Chemistry
University of Cambridge
Cambridge CB2 1EW, UK
E-mail: tpjk2@cam.ac.uk

R. P. B. Jacquat, D. Morse, Prof. T. P. J. Knowles
Cavendish Laboratory
University of Cambridge
Cambridge CB3 0HE, UK

Dr. D. Vigolo
School of Chemical Engineering
University of Birmingham
Edgbaston, Birmingham B15 2TT, UK

D. Morse
Division of Preclinical Innovation
National Center for Advancing Translational Sciences
National Institutes of Health
Bethesda, MD 20892, USA

The ORCID identification number(s) for the author(s) of this article can be found under https://doi.org/10.1002/smll.202000432



**DOI: 10.1002/smll.202000432**

Artificial analogues of the extracellular matrix (ECM) materials and their processing have been widely explored for tissue and organ engineering applications as well as for controlled drug release and disease models, which have the potential to reshape the future of regenerative, personalized, and precision medicine.[1–3] The miniaturization of bioactive protein hydrogels is a promising avenue for developing biocompatible and biomimetic micro reactors, cell-culture scaffolds, and building blocks for complicated structures in an efficient and highly controlled fashion.[4–7]

Native collagen is one of the main components of the ECM, and is commonly used as a key material for multiscale tissue and organ engineering studies as a result of its biocompatibility in the gel state.[8] However, the immunogenicity of certain types of collagen and their acidic-soluble nature have limited their extended applications.[8–11] In comparison, gelatin, consisting of the hydrolyzed or fragmented triple helical structures, has been widely used as a substitute for collagen, because gelatin has higher solubility at physiological pH, less immunogenicity, better formability or printability, simple transition between sol and gel states, cell adhesive Arg-Gly-Asp motifs inherited from collagen, and availability of scale.[12–17] With the tunable physical and chemical characteristics, gelatin is well accepted as artificial ECM materials for spatial or mechanical support for cells, coating layers, or as additives to other ECM composites to enhance cell adhesion and proliferation at the microscale (Table S1, Supporting Information).[12,18,19] Chemically crosslinked gelatin hydrogels are mechanically robust because of the presence of covalent bonds, but existing methods usually entail aldehydes or UV which can compromise the viability of cells or biomolecules.[20] Controlling the spatial organization of microgels through the physical or enzymatic crosslinking of gelatin under mild gelation conditions holds potential for biocompatible or thermostable artificial ECM materials without synthetic building blocks.[20–22]

There are two principal drivers for making spherical microgels with a controlled spatial distribution. First, native tissues are often inhomogeneous and anisotropic, and native ECM can have nonuniform mechanical properties, porosities, and interactions with cells.[23–27] Second, spherical microgels as biomimetic environments have larger specific surface areas for enhanced

possibilities for surface modifications and more uniform exchange of nutrients and metabolic waste products at each radial dimension at a small scale; for example, the diffusion distance of oxygen in tissues or spheroids is on average of the order of 200 µm.[28] Gelatin-based hydrogels have been fabricated at small scales with different 3D morphologies for biological purposes (Table S1, Supporting Information). Nevertheless, the existing gelatin microgels are mainly manufactured with UV or blue light illumination and include photoinitiators, material composites, or non-scalable techniques. Enzymatically crosslinked gelatin hydrogels have been used as microfluidic platforms for cell culture, but making monodispersed spherical microgels with density gradients is not well established.[29–31] We further note that enzymatically crosslinked gelatin offers potential for versatile crosslinking approaches and temperature control, opening up new possibilities to generate novel microgels with controlled conformation and spatial density of the gel (Table S1, Supporting Information). Physical and photocrosslinking of gelatin are usually faster than enzymatic crosslinking, as various crosslinking methods have different kinetics or rates, which could be exploited to regulate the structures of hydrogels at multiple scales in a time-sensitive manner.[32–34] In addition, microfluidic platforms could provide different flow patterns and droplet generation regimes, which can increase the structural diversity of the micron-scaled outcomes.[35–38]

The present study demonstrates a method to control the spatial distribution of structural proteins in spherical microgels through microfluidic control of mixing and physical and enzymatic crosslinking of gelatin under mild gelation conditions. Two inhomogeneous forms of gelatin microgels, microgels with a higher density in their cores (HDC) and microgels with a higher density in their shells (HDS), were fabricated via a gelatin-in-enzyme-in-oil (GEO) geometry and an enzyme-in-gelatin-in-oil (EGO) geometry, respectively, with an optimized microfluidic channel length. The HDC and HDS microgels had different dissolution rates when enzymatically dissolved, and the microgels also had different dissolution rates when exposed to varying concentrations of trypsin. These microgels are promising for further studies of gradient scaffolding materials for 3D cell culture, non-isotropic or position-independent cargo carriers with tailored release rates or degradability rates, and mini and soft environment with inhomogeneous or controllable mechanical or chemical properties.

We used a microfluidic setup in this study in combination with temperature control provided by a hot plate at 37 °C to keep the gelatin solution in its liquid state (**Figure 1**a). There were two inlets for the aqueous phases and one inlet for oil phase in the flow-focusing V-shaped microfluidic chip (Figures 1c and **2**c). Eight experiments (E1–E8) were performed in flow-focusing V-shaped junctions of microfluidic chips, the experimental conditions

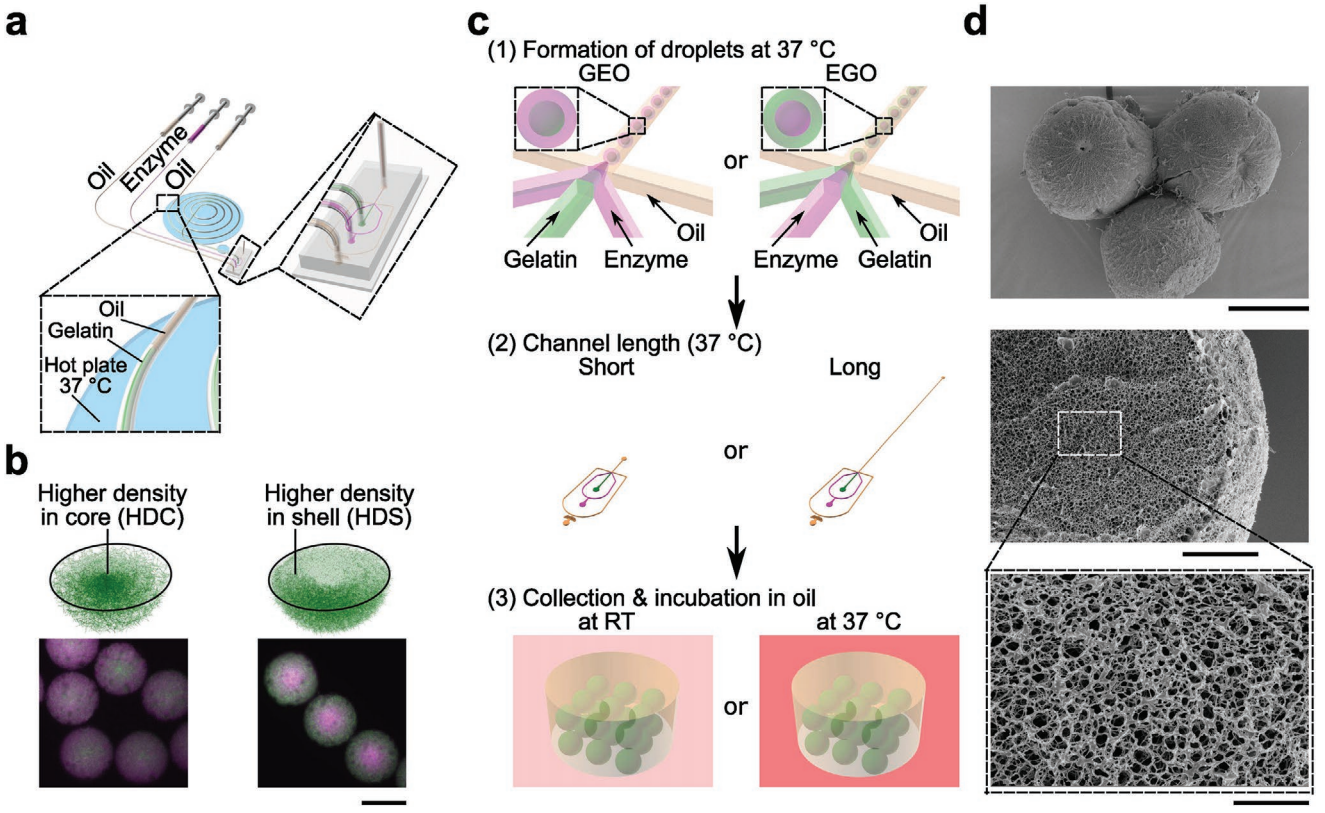


**Figure 1.** Formation of gradient protein microgels from gelatin. a) A microfluidic setup with associated heating elements. b) Cross-section schematics and fluorescent microscopy images of microgels with various radial density of gelatin hydrogel, including a higher density in their cores (HDC) and a higher density in their shells (HDS). Scale bar, 100 µm. c) The procedure and conditions of the formation of the microgels: (1) a gelatin-in-enzyme-in-oil (GEO) or enzyme-in-gelatin-in-oil (EGO) geometry at a flow-focusing V-shaped junction of a microfluidic chip, (2) a short or long channel, and (3) collection and incubation of microdroplets at RT or at 37 °C. d) Scanning electron microscopy (SEM) images of microgels through enzymatic crosslinking. Scale bar, 40 µm (upper), 10 µm (middle), and 2 µm (lower).

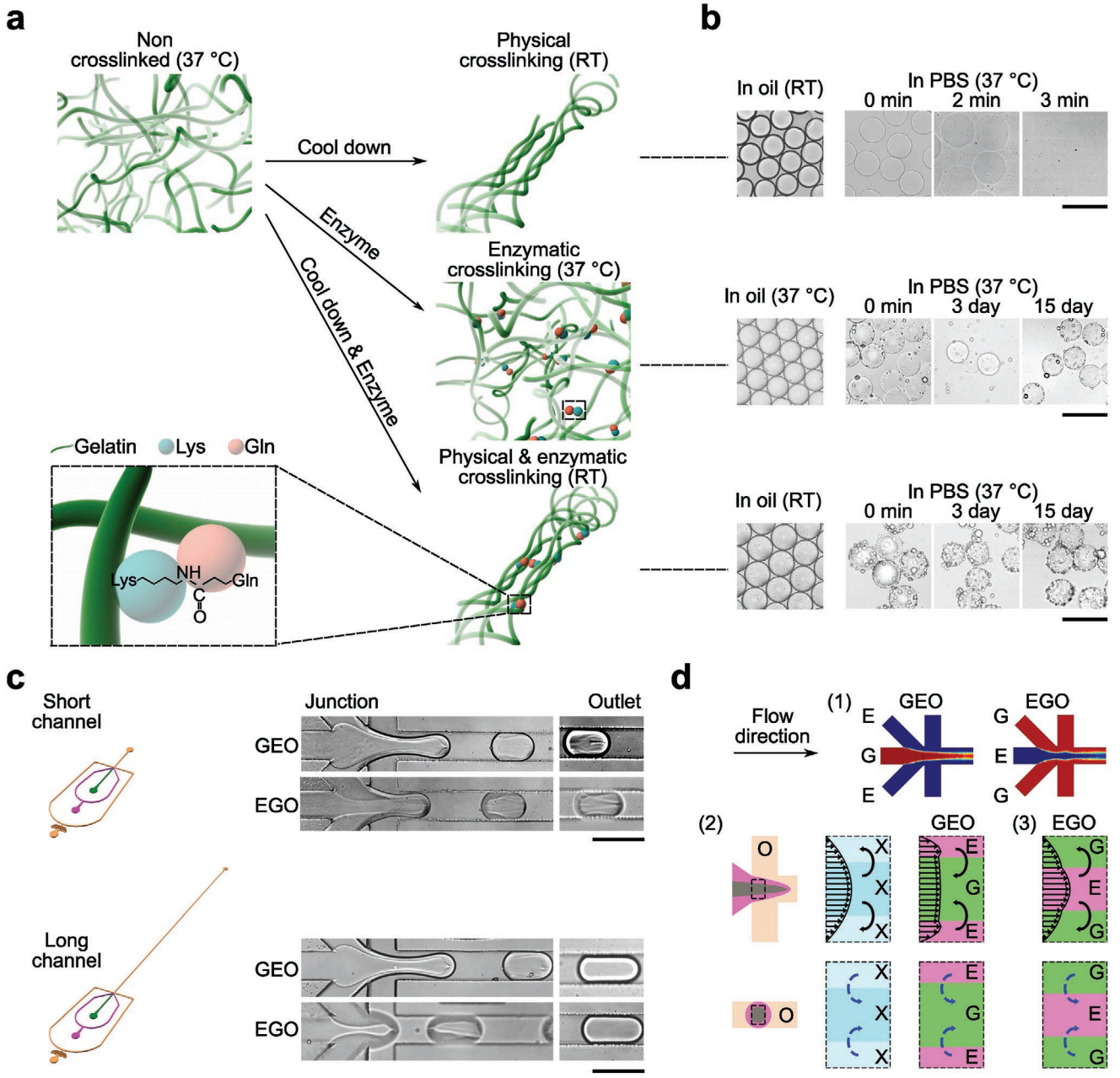


**Figure 2.** Crosslinking strategies and microfluidic mixing for the generation of gelatin microgels. a) Different crosslinking methods for the gelation of gelatin resulting in different molecular structures, including random coils in solution without crosslinking, triple helices in the gel state through physical crosslinking, interlinked random coils in the gel state through enzymatic crosslinking, and interlinked triple helices in the gel state through physical and enzymatic crosslinking. The gelatin molecular chains are connected by the covalent bonds between lysine (Lys) and glutamine (Gln) residues with transglutaminase through enzymatic crosslinking. b) Microscopy images of the thermostability studies of demulsified microgels in (a). Scale bar, 200 µm. c) The mixing of gelatin (G) and enzyme (E) solutions in the microdroplets in oil (O) near flow-focusing V-shaped junctions and near the outlets of the chips in short and long channels. Scale bar, 200 µm. d) (1) Finite element simulation of the distribution of gelatin and enzyme solutions at V-shaped flow-focusing junctions. (2) Top, recirculation flow at the junction of the GEO geometry is represented by the black curved arrows, and the black parallel arrows represent the velocities of liquids with different viscosities (X stands for a liquid such as water). Bottom, recirculation flow between the junction and the outlet of the GEO geometry is represented by the blue dashed curved arrows. (3) Top, recirculation flow at the junction of the EGO geometry. Bottom, recirculation flow between the junction and the outlet of the EGO geometry. The flow direction in (d) is toward the outlet.

include: 1) formation of droplets at 37 °C via a GEO geometry or an EGO geometry, 2) in short channels or long channels of microfluidic chips at 37 °C, and 3) collection and incubation of droplets in oil at room temperature (RT; 25 °C) or 37 °C (Figure 1c).

Previously, bulk studies showed the physical and enzymatic crosslinking of gelatin for cell-culture purposes, and the connection of lysine and glutamine residues in the presence of transglutaminase (**Figure** 2a).[21] A gelatin solution underwent a

sol–gel transition when cooled down below 36 °C through physical crosslinking (Figure 2a).[39] By contrast, enzymatic crosslinking would stabilize a gelatin solution at 37 °C or higher, and a combined gelation through physical and enzymatic crosslinking took place below 36 °C.[39] As such, the molecular structures of microgels obtained after physical and enzymatic crosslinking (E1–E4) were crosslinked triple helices when microdroplets were collected and incubated at RT (Figures 2a and **3**a), while the molecular structures of microgels through only enzymatic crosslinking (E5–E8) were crosslinked random coils when microdroplets were collected and incubated at 37 °C (Figures 2a and 3b). All microgels (E1–E8) were not made at non-physiological temperatures, and thus possibilities could be explored for the encapsulation of living cells and heat-labile biomolecules or drugs.

The microgels (E1–E8) were thermostable at 37 °C in phosphate buffered saline (PBS) solution for at least 15 days, and no visible shrinkage or swelling of the microgels was observed during the incubation in oil, the demulsification into PBS, or the following thermostability study in PBS (Figure 2b and Figures S2 and S3, Supporting Information). This indicated the structural stability of microgels (E1–E8) caused by the robust covalent bonds (Figure 2a,b). Some microdroplets (E5–E8) shrank when collected and incubated in oil at 37 °C because of the evaporation of water, and these microgels did not expand to original size after demulsification, further indicating the structural stability of microgels caused by robust covalent bonds (Figure 2b and Figure S3, Supporting Information). Robust networks and nanopores of protein hydrogels were presented, and the macro- and microstructures were preserved during the fast freezing-drying process (Figure 1d). These porous microgels could support cell growth and allow the exchange of nutrition and metabolic wastes in 3D. The design principles of the microgels are promising for making multifunctional and thermostable ECM environments at physiological conditions.

A control experiment shows that physically crosslinked microgels (E0) dissolved rapidly at 37 °C in PBS with noticeable size expansion of the microgels, though they could also be manufactured monodispersedly at 37 °C in microfluidic chips and remained stable at RT in aqueous solution (Figure 2b and Figure S5, Table S2, Supporting Information). Owing to the weak physical crosslinking, water molecules could easily penetrate into the microgels during the demulsification at RT and the incubation at 37 °C and caused the swelling of the microgels. The rapid dissolution of physically crosslinked microgels at 37 °C indicated that the sol–gel transition of physical gelation is reversible, because the conversion from single-stranded coil structures to triple helical structures is based on weak intermolecular forces such as hydrogen bonds, van der Waals forces, electrostatic or hydrophobic interactions (Figure 2a).[40–42] Although gelatin-based composites were commonly used to increase the mechanical property and thermal instability of gels, the addition of other materials such as alginate and chitosan could introduce non-protein or non-mammalian cell components which might cause more inflammatory responses for further studies in vivo (Table S1, Supporting Information).[43] Compared to strengthened gelatin via synthesis, the gelatin in this present study did not introduce non-collagen radicals or non-biological functional groups or hinder the conformation of triple helical structures, and thus more closely resembled native collagen gel (Table S1, Supporting Information). Previous studies showed the viability of cells cultured in and on enzymatically crosslinked gelatin in bulk.[21,29,44–46] The microgels in this present study could therefore find applications as implantable grafts or vehicles encapsulating cells. Photocrosslinked gelatin is increasingly popular in regenerative medicine because of the rapid gelation and relative biocompatibility.[47] There are however challenges regarding the use of UV, photoinitiators, and methacrylate groups for cell studies.[48,49] Without UV, gelatin is more inclined to gel physically at room temperature than photocrosslinkable gelatin; this tendency of physical gelation makes gelatin suitable for high-throughput generation of microgels in combination with enzymatic crosslinking (Table S1, Supporting Information).[47]

We next set out to explore whether we could modulate the radial distribution of protein gel within the microgels by seeking to control the mixing of the aqueous streams on chip. Two main fluid behavior factors influence the mixing of multi aqueous phases in microdroplets. The first factor is the recirculation flow in microdroplets between the junction and the outlet. It has been known that this phenomenon is caused by the shearing interactions of the fluids in the microdroplets with the stationary walls.[37,38] Longer channels and smaller microdroplets would enhance this recirculation flow and the mixing of multi aqueous phases.[37,38] It is therefore expected that shortening the channel length would result in the better preservation of the initial spatial positions of the two aqueous phases in droplets. The second factor is the recirculation flow in microdroplets at the junction. This phenomenon is caused by different velocities of the adjacent liquids as a result of the Hagen–Poiseuille law and the interior properties of the multiple aqueous solutions, and exists at the flow-focusing junctions during or shortly after the formation of the microdroplets.[50]

The radial density of microgels could be affected by the channel lengths during the dynamic mixing of the gelatin and enzyme solutions caused by the two forms of recirculation flows mentioned above (Figure 2c,d). Among the eight experiments (E1–E8), HDC and HDS microgels were obtained when the microdroplets were made at 37 °C in short channels and then collected and incubated at RT (E1 and E2 in **Figure 3**a). Microgels with homogeneous density (HmD) were also made (E3–E8 in Figure 3a,b). The structural differences of microgels were indicated by the green nanospheres (GNSs) pre-mixed in gelatin solution and red nanospheres (RNSs) pre-mixed in enzyme solution with 2D fluorescent microscopy (Figure 3a). 3D confocal microscopy further showed that the GNSs peaked at the centre of the HDC microgels (E1) but peaked near the edge of the HDS microgels (E2), while HmD microgels (E3–E8) did not have a particular peak of the GNSs along the radius (Figure 3d,e and Figures S7–S9, Supporting Information). The HDC and HDS microgels could function as inhomogeneous micro-ECM environment with gradient gel distribution, varying stiffness, and diversified porosities and permeabilities.[23–27] To manufacture building blocks for artificial tissues or complex organ precursors, multiple cells in intricate patterns or compartmentalised alignment are usually needed.[15] The microgels are promising to serve these purposes of 3D cell mono-culture or co-culture scenarios with controllable anisotropic micro environment, which might lead to varying cell fates and varying diffusion of nutrients or growth factors.

GEO and EGO geometries were used to make HDC and HDS microgels respectively (E1 and E2; Figure 1b,c). The interfaces between the gelatin the enzyme solutions before the formation of the microdroplets indicated the laminar flows of the two aqueous solutions (Figure 2c). The radial density of microgels first depended on the initial spatial positions of the two aqueous inherited from the laminar flow before the V-shaped junction, and then depended on the degree to which these positions were preserved after the junction. Shortening the channel length has been proved to be an effective method to make inhomogeneous microgels (E1 and E2). Obviously, there was more gelatin in the microgel cores via the GEO geometry and more gelatin in the shells via the EGO geometry shortly after the formation of the microdroplets at the junction, followed by the

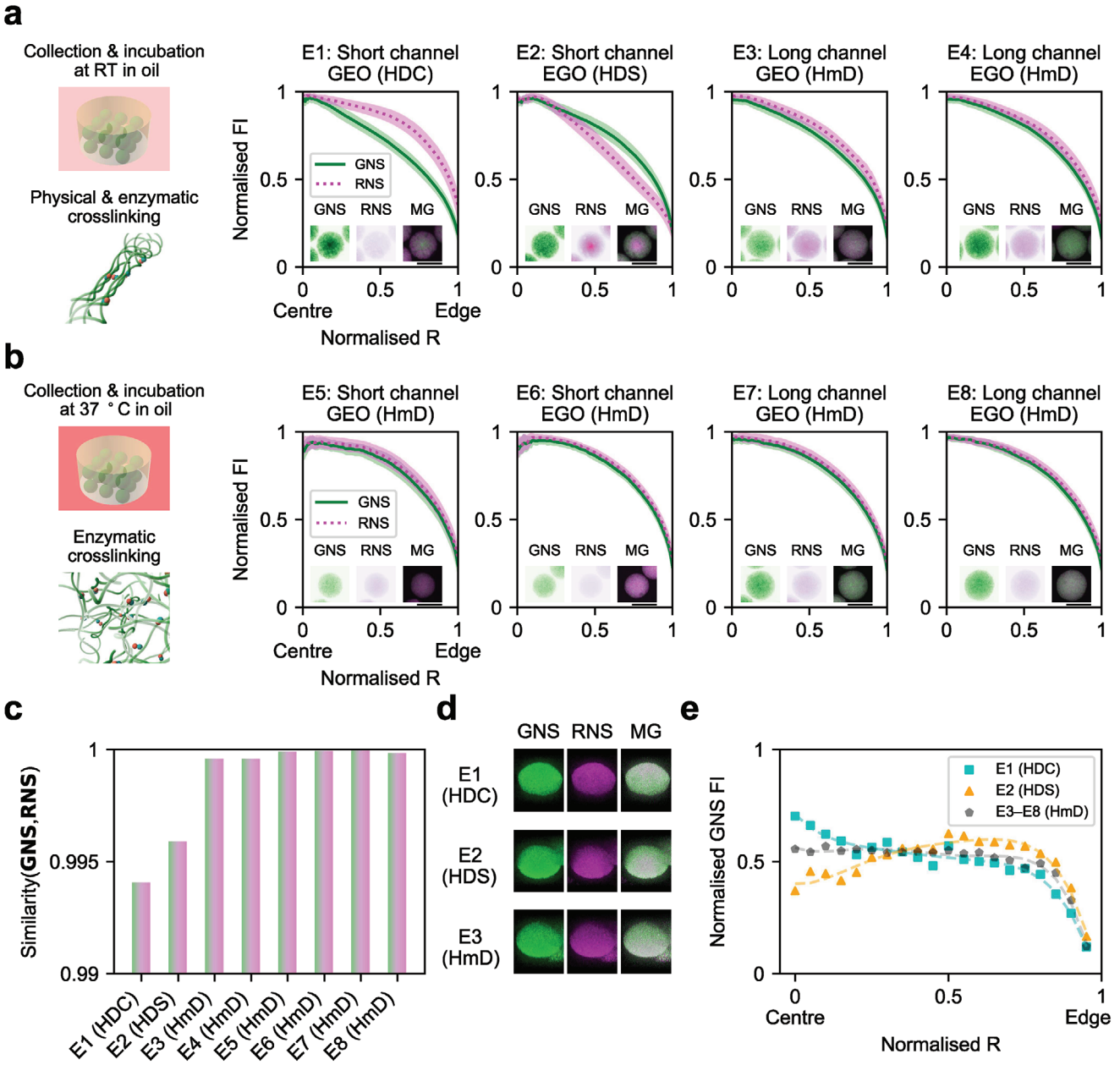


**Figure 3.** Radial density distribution of the gelatin microgels. a,b) 2D fluorescent microscopy images and the analyses of the radial density of the microgels after demulsification. The microdroplets were previously collected and incubated at RT (a) or at 37 °C (b) in oil. The normalized fluorescent intensity (FI) was the mean value of the FI of green nanospheres (GNSs) pre-mixed in gelatin solution and red nanospheres (RNSs) pre-mixed in enzyme solution along the normalized radius (R) in concentric rings of 2D images of microgels. Standard deviations are shown in the plots. Sample size by autodetection in (a,b) was 239, 198, 244, 250, 57, 108, 131, and 90 (E1 to E8). Scale bar, 100 μm. c) Cosine similarity of radial vector **GNS** and radial vector **RNS**. Similarity (**GNS**,**RNS**) = cos (**GNS**,**RNS**). Higher similarity (**GNS**,**RNS**) means higher similarity or smaller angle between **GNS** and **RNS**. d) 3D confocal microscopy images of HDC, HDS, and HmD microgels. e) Normalized FI of GNSs pre-mixed in gelatin solution along the normalized R in concentric rings of the middle layer of 3D confocal microscopy images in HDC, HDS, and HmD microgels. Polynomial fittings (power 5) are shown by dashed lines in the plots.

mixing and mutual diffusion of the two aqueous phases. The recirculation flow between the junction and the outlet and the flow of droplets are shown in Figure 2d. There was sharper visible phase contrast of gelatin and enzyme solutions at the outlets in short channels than long channels, indicating that the two aqueous solutions were less mixed in short channels (Figure 2c and Figure S10, Supporting Information). Therefore, the HDC and HDS structures survived the recirculation flow between the junction and the outlet in short channels, which agrees with the radial distribution of GNSs and RNSs in the HDC and HDS microgels (Figure 3a,b,e and Figures S7–S9, Supporting Information).

We used long straight channels (Figures 2c,d and 3a,b), complementing previous studies which showing the winding channels could function as oscillators to enhance the mixing of liquids in microdroplets at each turns.[36] Previous studies reported that that two aqueous reagents of differing viscosities may mix more rapidly than two aqueous reagents with matched viscosities.[51] In this present study, the ratio of dynamic viscosity of gelatin solution to that of enzyme solution was around 13:1, and thus it is inferred that mixing of gelatin and enzyme solutions is quicker than mixing two same liquids such as two gelatin solutions in microfluidic channels. The long channels we used were enough to well mix the gelatin and enzyme solutions quickly.

Recirculation flow at the junction could also influence the mixing of the aqueous solutions in the microdroplets. At the junctions of the microfluidic chips, the interfaces of gelatin and enzyme solutions bent from the gelatin solution to enzyme solution (Figure 2c,d), indicating the higher liquid pressure of gelatin solution resulted from the higher viscosity of the gelatin solution when the two aqueous solutions had same flow rates (Figure S11, Supporting Information). The different viscosities of the gelatin and enzyme solutions led to the different velocities of these two solutions in microfluidic channels and thus led to the recirculation flow at the junction when the microdroplets were newly formed (Figure 2d). The direction of recirculation flow at the junction of GEO geometry is opposite to the direction of the recirculation flow between the junction and the outlet of the GEO geometry, while the directions of those two recirculation flows of the EGO geometry are the same (Figure 2d). It is thus expected that there was more mixing in the EGO geometry (E2) than GEO geometry (E1), which agrees with the similarity (**GNS**,**RNS**) (Figure 3c) and the average square difference (Figure S6a, Supporting Information). Recirculation flow between the junction and the outlet and recirculation flow at the junction were both complex in the dynamic microdroplets. In long channels (Figure 2c), the recirculation flow between the junction and the outlet prevailed over the recirculation flow at the junction, and the gelatin and enzyme solutions were totally mixed in the microgels which agreed with the similarity (**GNS**,**RNS**) (Figure 3a–c) and the similarity (**GM**,**RM**) (Figures S8c and S9c, Supporting Information).

In general, the formation of the HDC and HDS microgels (Figures 1b,c and 3a) can be distinguished by the following three steps: 1) the HDC and HDS structures were formed, respectively, via GEO and EGO geometries, because the mixing of gelatin and enzyme solutions was insufficient during the formation of microdroplets in short microfluidic channels at 37 °C (Figures 2c,d and 3a); then 2) the HDC and HDS structures were immediately stabilized through physical crosslinking during the collection and incubation of microdroplets at RT in oil (Figures 2a and 3a); then 3) the physically crosslinked HDC and HDS structures were gradually stabilized through enzymatic crosslinking when microdroplets were incubated at RT in oil (Figures 2a and 3a). The physical crosslinking of gelatin started immediately in the tubing (off-chip) when microdroplets were cooled down to RT, but the enzymatic crosslinking was relatively slow and gradual and might last several hours.[32] Collecting and incubating the microdroplets at 37 °C in oil means there was no physical crosslinking to quickly stabilize the inhomogeneous structures formed in short channels, and the diffusion and mixing of the two aqueous phases caused HmD microgels (Figures 2a and 3b).

The dissolution of HDC microgels through enzymolysis was faster than that of HDS microgels, which indicated that HDC microgels were more porous in the periphery than HDS microgels and further highlighted the structural difference of them (Figures 1b and **4**a,b). The dissolution of HDS microgels with various concentrations of trypsin is also shown (**Figure 4**c,d). Trypsin can cleave C-terminal to arginine and lysine of protein.[52] With decreasing concentration of trypsin (C1–C9), slower dissolution of the microgels was observed in terms of later dissolution starting time and longer dissolution duration (Figure 4c,d). Quite understandably, higher concentration of trypsin means an increasing rate at which enzyme (trypsin) and substrate molecules (gelatin) encounter one another according to Michaelis–Menten kinetics. Both the internal structures of the microgels and the external environments could affect the degradability rates of the microgels.

These dissolvable microgels could be used to build environmentally sensitive, biodegradable, and transparent soft robotic structures with a pre-set life expectancy.[53] Protein hydrogels can be degraded via enzymolysis with trypsin, matrix metallopeptidase, or collagenase, but it is not well known that enzymes secreted by mammals could digest polysaccharides such as alginate.[15,54] On the one hand, the degradation of ECM materials is a critical cellular and physiological process related to growing and diseases, and it would be necessary to build in vitro disease models such as 3D cancer models with degradable ECM materials to better mimic their natural counterparts.[53,54] On the other hand, one goal of 3D tissue models is to create soft and smart implants in vivo, and thus the artificial ECM materials should be weakened or degraded at some point after the transplant so that the cells in 3D tissue models could better adapt to the physiological conditions in vivo and better connect to the hosts. The distinctively different dissolution behaviors of HDC and HDS microgels indicate that they could apply to in vitro or in vivo tissue models with tailored degradability in a temporal manner. The use of nanospheres represents not only the density of the gelatin, but also the spatial position and the release of nanoparticles, which is promising for controllable or gradually degradable nanoparticle-based drug carriers in precision medicine therapies.[55,56]

By harnessing the physicochemical properties of gelatin and the fluid dynamics in microfluidic channels, this study presents an approach to control the radial density of protein-only microgels at mild gelation conditions. GEO and EGO microfluidic methods were, respectively, adopted to make HDC and HDS

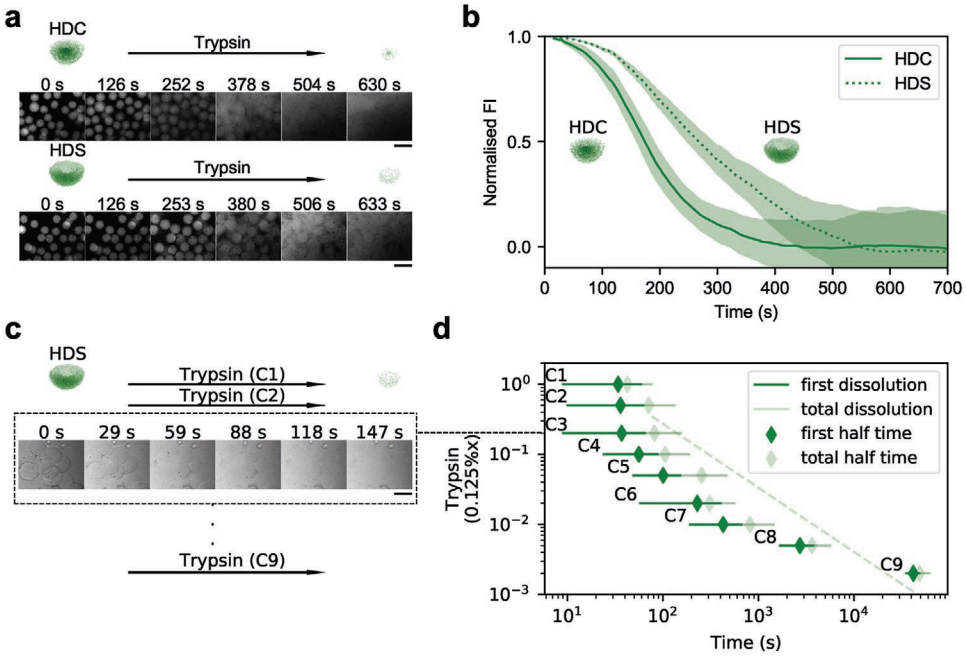


**Figure 4.** Dissolution of gelatin microgels through enzymatic digestion. a) Time-lapse microscopy images showing the dissolution process of HDC and HDS microgels. The GNSs were pre-mixed in gelatin solution and stabilized in the microgels. Scale bar, 200 µm. b) The normalized average fluorescent intensity (FI) of GNSs in the microgel areas in (a). Standard deviations are shown in the plots. More than 60 HDC microgels and more than 60 HDS microgels were autodetected. c) The time-lapsed images of HDS microgels dissolved with diminishing concentrations (C1–C9) of trypsin. Scale bar, 100 µm. d) The dissolution duration of the HDS microgels in (c).

microgels. HDC and HDS microgels survived the recirculation flows in the microdroplets with optimized microfluidic channel length at tuned temperature. HDC and HDS microgels showed different dissolution rates of the microgels through enzymolysis. The microgels were generated in a robust, simple, and biocompatible fashion in this study, and the use of enzyme (transglutaminase) led to the thermostability of microgels because of the robust covalent bonds. These controllable and degradable microgels hold potential for inhomogeneous or gradient reactors for applications in 3D cell-culture scaffolds, regeneration of artificial tissues or organs in vitro, implants or drug carries in vivo, controlled release of molecules, mechanical property testing of mini-ECM hydrogels, and as soft building blocks of complex and nature-inspired robots.

## Experimental Section

*Materials Preparation*: Gelatin solution (100 mg mL$^{-1}$) was made by dissolving gelatin powder (Sigma-Aldrich Co Ltd, MO, US; product of Germany) in PBS (Oxoid Ltd, Hampshire, UK) at 50 °C with magnetic stirring for 2 h. Enzyme solution, that is, transglutaminase solution (50 mg mL$^{-1}$), was made by dissolving transglutaminase powder (Special Ingredients Ltd, Chesterfield, UK; product of Spain) in PBS at RT for 2 h, and the solution was filtrated with a 0.22 µm filter. Gelatin solution and enzyme solution were then kept at 4 °C and used within 1 week. GNSs (200 nm, 1% solids, Fluoro-Max, Thermo Scientific, CA, US) were pre-mixed in the gelatin solution (1/50, v/v). RNSs (100 nm, 1% solids, Fluoro-Max, Thermo Scientific, CA, US) were pre-mixed in enzyme solution (1/50, v/v). Fluorosurfactant (2%, w/w) (RAN Biotechnologies, MA, US) was dissolved in Fluorinert (FC-40)(TM) (Reg) (Fluorochem, Hadfield, UK) (1/50, v/v) as the continuous phase of emulsion.

*Microgel Formation*: Microfluidic devices were fabricated by soft lithography techniques as previously reported.[57] 1) Flow-focusing V-shaped microfluidic chips were used to make crosslinked gelatin microgels with enzyme. The height and width of the microfluidic channels were 50 and 100 µm, respectively; the channel length between the junction and the outlet of short and long channels were 3340 and 33400 µm, respectively (Figure S12, Supporting Information). Gelatin solution, enzyme solution, and FC-40 with surfactants were loaded in three separate syringes with polythene tubings. The tubing containing gelatin solution was fixed on a hot plate (MS-H280-Pro, Camlab, Cambridge, UK) at 37 °C with adhesive tapes, and an additional small temperature-controlled sheet (Warner Instruments, Model TC-124A, CT, US) was also be set at 37 °C to prevent the gelation of gelatin in the tubing. The flow rates of gelatin solution, enzyme solution, and FC-40 with surfactants were respectively set at 100, 100, and 400 µL h$^{-1}$ with a digital neMESYS pump system (CETONI GmbH, Korbussen, Germany). The microdroplets were formed at the flow-focusing V-shaped junctions of the microfluidic chips at 37 °C, and were then collected and overnight incubated in Eppendorf tubes at RT or at 37 °C for different studies. The gelatin then became crosslinked microgels, which were then demulsified with 10% 1H,1H,2H,2H-perfluoro-1-octanol (Sigma-Aldrich Co Ltd, MO, US) and finally rinsed with PBS.[58] 2) Flow-focusing single-T microfluidic chips were used to make physically crosslinked gelatin microgels without enzyme. The height and width of the microfluidic channels were 50 and 100 µm, respectively (Figure S5, Supporting Information). Gelatin solution and FC-40 with surfactants were loaded in two separate syringes with polythene tubings. The microdroplets were formed at the flow-focusing single-T junctions of the microfluidic chips at 37 °C, and were then collected and overnight incubated in Eppendorf tubes at RT. The microgels were demulsified with 10% 1H,1H,2H,2H-perfluoro-1-octanol at RT or lower temperature. 1H,1H,2H,2H-perfluoro-1-octanol was kept in fumehood.

*Optical Microscopy*: 1) The bright-field images of the formation of microdroplets were taken with a high-speed camera (MotionBLITZ EoSens Mini1-1 MC1370, Mikrotron, Unterschleissheim, Germany) on a microscope (Oberver.A1, Axio, Zeiss, Oberkochen, Germany). The dark-field

fluorescent images of the microgels were taken with a CCD camera (CoolSNAP MYO, Photometrics, AZ, US) on a microscope (Oberver. A1, Axio, Zeiss, Oberkochen, Germany); for the GNSs and RNSs, a 49001 filter (excitation wavelength 426–446 nm, emission wavelength 460–500 nm) and a 49004 filter (excitation wavelength 532–557 nm, and emission wavelength 570–640 nm) were, respectively, used with a compact light source (HXP 120 V, Leistungselektronik Jena GmbH, Jena, Germany). 2) Confocal images were taken on a confocal microscope (Leica TCS SP5, Germany) for GNSs (excitation wavelength 468 nm, emission wavelength 508 nm) and RNSs (excitation wavelength 542 nm, and emission wavelength 612 nm). Data were analyzed with Python and ImageJ.

*Scanning Electron Microscopy (SEM)*: 1) Critical point drying principles were used to remove the ethanol. Microgels in PBS was dehydrated with 25%, 50%, 75%, 80%, 90%, and 100% ethanol. The microgels were then coated with platinum and observed in an SEM microscope (FEI Verios 460, Thermo Fisher). 2) A fast freezing-drying method was also used to make SEM samples; microgels were rinsed in liquid ethane, and the liquid ethane then evaporated in $CO_2$ gas environment. The microgels were then coated with platinum and observed in the same SEM microscope. HV = 2.00 kV. Current = 25 pA.

*Dissolution*: 1) Trypsin (concentration 0.25%) (Life Technologies Ltd, Paisley, UK) was added to HDC and HDS microgels with green fluorescent nanospheres in PBS (1/1, v/v) in a 96-well UV-transparent half-area plate; the dark-field fluorescent time-lapse images were taken with a CCD camera (CoolSNAP MYO, Photometrics, AZ, US) on a microscope (Oberver.A1, Axio, Zeiss, Oberkochen, Germany) with a 49001 filter (excitation wavelength 426–446 nm, emission wavelength 460–500 nm) to observe the GNSs. 2) Trypsin (original concentration 0.25%) was diluted by a factor of 1, 2, 5, 10, 20, 50, 100, 200, and 500, and trypsin with each of these concentrations (C1–C9) was added to the HDS microgels in PBS (1/1, v/v) in a 96-well UV-transparent half-area plate (Corning Incorporated, ME, US); and the bright-field time-lapse images of the dissolution of microgels were taken with a CCD camera (CoolSNAP MYO, Photometrics, AZ, US) on a microscope (Oberver.A1, Axio, Zeiss, Oberkochen, Germany).

*Dynamic Viscosity Testing*: A microfluidic pressure controller (OB1 MK3, Paris, France) was used to test the relative viscosities of gelatin solution, enzyme solution, FC-40 with surfactants, and PBS at 37 °C. These four solutions were loaded, respectively, into tubings with same length and diameter, and the volumes of the four liquids were collected and calculated when they were pushed by the pneumatic pump for 5 min. The dynamic viscosities of the four liquids are inversely proportional to the volumes of the liquids collected. The ratio of the dynamic viscosities of gelatin solution, enzyme solution, FC-40 with surfactants, and PBS is roughly estimated to be 19.94:1.53:2.99:1. The results of dynamic viscosity testing were used for COMSOL simulation.

*COMSOL Simulation*: COMSOL Multiphysics 5.2a was used to perform the simulations of the microfluidic flow-focusing junction. A 2D coupled laminar flow and transport of diluted species physics were used to simulate the inter-diffusion of the two miscible phases after the junction and to obtain the viscosity and velocity profiles.

## Supporting Information

Supporting Information is available from the Wiley Online Library or from the author.

## Acknowledgements

The research leading to these results had received funding from the Cambridge Trust (Y.X.), the Jardine Foundation (Y.X.), Trinity College Cambridge (Y.X.), the Engineering and Physical Sciences Research Council Centre for Doctoral Training in Sensor Technologies and Applications (EP/L015889/1; R.P.B.J.), the BBSRC (T.P.J.K.), the Newman Foundation (T.P.J.K.), the Wellcome Trust (T.P.J.K.), and the European Research Council under the European Union's Seventh Framework Programme (FP7/2007-2013) through the ERC grant PhysProt (agreement no. 337969; T.P.J.K.).

Note: Ref. [7] was updated on 13 August 2020 after original online publication.

## Conflict of Interest

The authors declare no conflict of interest.

## Keywords

enzymatic crosslinking, gelatin, microfluidic mixing, microgels, physical crosslinking, radial density

Received: January 21, 2020
Revised: April 20, 2020
Published online: June 11, 2020

[1] B. Zhang, A. Korolj, B. F. L. Lai, M. Radisic, *Nat. Rev. Mater.* **2018**, 1.
[2] P. Zorlutuna, N. Annabi, G. Camci-Unal, M. Nikkhah, J. M. Cha, J. W. Nichol, A. Manbachi, H. Bae, S. Chen, A. Khademhosseini, *Adv. Mater.* **2012**, *24*, 1782.
[3] A. Kamada, A. Levin, Z. Toprakcioglu, Y. Shen, V. Lutz-Bueno, K. N. Baumann, P. Mohammadi, M. B. Linder, R. Mezzenga, T. P. J. Knowles, *Small* **2019**, 1904190.
[4] S. N. Bhatia, D. E. Ingber, *Nat. Biotechnol.* **2014**, *32*, 760.
[5] T. P. J. Knowles, R. Mezzenga, *Adv. Mater.* **2016**, *28*, 6546.
[6] U. Shimanovich, F. S. Ruggeri, E. De Genst, J. Adamcik, T. P. Barros, D. Porter, T. Müller, R. Mezzenga, C. M. Dobson, F. Vollrath, C. Holland, T. P. J. Knowles, *Nat. Commun.* **2017**, *8*, 15902.
[7] Y. Shen, F. S. Ruggeri, D. Vigolo, A. Kamada, S. Qamar, A. Levin, C. Iserman, S. Alberti, P. S. George-Hyslop, T. P. J. Knowles, *Nat. Nanotechnol.* **2020**, https://doi.org/10.1038/s41565-020-0731-4.
[8] R. Parenteau-Bareil, R. Gauvin, F. Berthod, *Materials* **2010**, *3*, 1863.
[9] C. Bertulli, M. Gerigk, N. Piano, Y. Liu, D. Zhang, T. Müller, T. P. J. Knowles, Y. Y. S. Huang, *Sci. Rep.* **2018**, *8*, 12480.
[10] B. Chevallay, D. Herbage, *Med. Biol. Eng. Comput.* **2000**, *38*, 211.
[11] C. Yang, P. J. Hillas, J. A. Báez, M. Nokelainen, J. Balan, J. Tang, R. Spiro, J. W. Polarek, *Biodrugs* **2004**, *18*, 103.
[12] K. Yue, G. Trujillo-de Santiago, M. M. Alvarez, A. Tamayol, N. Annabi, A. Khademhosseini, *Biomaterials* **2015**, *73*, 254.
[13] S. Gnavi, L. di Blasio, C. Tonda-Turo, A. Mancardi, L. Primo, G. Ciardelli, G. Gambarotta, S. Geuna, I. Perroteau, *J. Tissue Eng. Regen. Med.* **2017**, *11*, 459.
[14] S. Sant, D. F. Coutinho, A. K. Gaharwar, N. M. Neves, R. L. Reis, M. E. Gomes, A. Khademhosseini, *Adv. Funct. Mater.* **2017**, *27*, 1606273.
[15] Y. Xu, X. Wang, *Biotechnol. Bioeng.* **2015**, *112*, 1683.
[16] Y. Xu, D. Li, X. Wang, in *Organ Manufacturing* (Ed: X. Wang), Nova Science Publishers Inc., Hauppauge, NY **2015**, pp. 245–268.
[17] Y. Xu, D. Li, X. Wang, in *Organ Manufacturing* (Ed: X. Wang), Nova Science Publishers Inc., Hauppauge, NY **2015**, pp. 201–225.
[18] L. Gibot, T. Galbraith, J. Bourland, A. Rogic, M. Skobe, F. A. Auger, *Nat. Protoc.* **2017**, *12*, 1077.
[19] J. Oh, K. Kim, S. W. Won, C. Cha, A. K. Gaharwar, Š. Selimović, H. Bae, K. H. Lee, D. H. Lee, S.-H. Lee, A. Khademhossenni, *Biomed. Microdevices* **2013**, *15*, 465.
[20] B. J. Klotz, D. Gawlitta, A. J. Rosenberg, J. Malda, F. P. Melchels, *Trends Biotechnol.* **2016**, *34*, 394.
[21] C. W. Yung, L. Q. Wu, J. A. Tullman, G. F. Payne, W. E. Bentley, T. A. Barbari, *J. Biomed. Mater. Res. A* **2007**, *83*, 1039.

[22] S. Das, F. Pati, Y.-J. Choi, G. Rijal, J.-H. Shim, S. W. Kim, A. R. Ray, D.-W. Cho, S. Ghosh, *Acta Biomater.* **2015**, *11*, 233.
[23] B. M. Gillette, J. A. Jensen, B. Tang, G. J. Yang, A. Bazargan-Lari, M. Zhong, S. K. Sia, *Nat. Mater.* **2008**, *7*, 636.
[24] B. M. Gillette, N. S. Rossen, N. Das, D. Leong, M. Wang, A. Dugar, S. K. Sia, *Biomaterials* **2011**, *32*, 8067.
[25] E. Melo, N. Cárdenes, E. Garreta, T. Luque, M. Rojas, D. Navajas, R. Farré, *J. Mech. Behav. Biomed. Mater.* **2014**, *37*, 186.
[26] J. J. Tomasek, J. E. Mazurkiewicz, S. A. Newman, *Dev. Biol.* **1982**, *90*, 118.
[27] A. Malandrino, M. Mak, R. D. Kamm, E. Moeendarbary, *Extreme Mech. Lett.* **2018**, *21*, 25.
[28] K. Alessandri, B. R. Sarangi, V. V. Gurchenkov, B. Sinha, T. R. Kießling, L. Fetler, F. Rico, S. Scheuring, C. Lamaze, A. Simon, S. Geraldo, D. Vignjević, H. Doméjean, L. Rolland, A. Funfak, J. Bibette, N. Bremond, P. Nassoy, *Proc. Natl. Acad. Sci. USA* **2013**, *110*, 14843.
[29] A. L. Paguirigan, D. J. Beebe, *Nat. Protoc.* **2007**, *2*, 1782.
[30] A. Paguirigan, D. Beebe, *Lab Chip* **2006**, *6*, 407.
[31] S. Hou, R. Lake, S. Park, S. Edwards, C. Jones, K. J. Jeong, *ACS Appl. Bio Mater.* **2018**, *1*, 1430.
[32] H. J. Bae, D. O. Darby, R. M. Kimmel, H. J. Park, W. S. Whiteside, *Food Chem.* **2009**, *114*, 180.
[33] A. I. Van Den Bulcke, B. Bogdanov, N. De Rooze, E. H. Schacht, M. Cornelissen, H. Berghmans, *Biomacromolecules* **2000**, *1*, 31.
[34] S. R. Shin, C. Zihlmann, M. Akbari, P. Assawes, L. Cheung, K. Zhang, V. Manoharan, Y. S. Zhang, M. Yüksekkaya, K.-T. Wan, M. Nikkhah, M. R. Dokmeci, X. S. Tang, A. Khademhosseini, *Small* **2016**, *12*, 3677.
[35] E. V. Yates, T. Müller, L. Rajah, E. J. De Genst, P. Arosio, S. Linse, M. Vendruscolo, C. M. Dobson, T. P. J. Knowles, *Nat. Chem.* **2015**, *7*, 802.
[36] J. Hong, M. Choi, J. B. Edel, A. J. deMello, *Lab Chip* **2010**, *10*, 2702.
[37] J. D. Tice, H. Song, A. D. Lyon, R. F. Ismagilov, *Langmuir* **2003**, *19*, 9127.
[38] K. Handique, M. A. Burns, *J. Micromech. Microeng.* **2001**, *11*, 548.
[39] J. Peyrelasse, M. Lamarque, J. Habas, N. El Bounia, *Phys. Rev. E* **1996**, *53*, 6126.
[40] H. Babin, E. Dickinson, *Food Hydrocoll.* **2001**, *15*, 271.
[41] C. Peña, K. De La Caba, A. Eceiza, R. Ruseckaite, I. Mondragon, *Bioresour. Technol.* **2010**, *101*, 6836.
[42] N. Holten-Andersen, M. J. Harrington, H. Birkedal, B. P. Lee, P. B. Messersmith, K. Y. C. Lee, J. H. Waite, *Proc. Natl. Acad. Sci. USA* **2011**, *108*, 2651.
[43] F. Sampaziotis, A. W. Justin, O. C. Tysoe, S. Sawiak, E. M. Godfrey, S. S. Upponi, R. L. Gieseck, III, M. C. de Brito, N. L. Berntsen, M. J. Gómez-Vázquez, D. Ortmann, L. Yiangou, A. Ross, J. Bargehr, A. Bertero, M. C. F. Zonneveld, M. T. Pedersen, M. Pawlowski, L. Valestrand, P. Madrigal, N. Georgakopoulos, N. Pirmadjid, G. M. Skeldon, J. Casey, W. Shu, P. M. Materek, K. E. Snijders, S. E. Brown, C. A. Rimland, I. Simonic, et al., *Nat. Med.* **2017**, *23*, 954.
[44] J. Sun, Y. Ren, W. Wang, H. Hao, M. Tang, Z. Zhang, J. Yang, Y. Zheng, X. Shi, *ACS Biomater. Sci. Eng.* **2020**, *6*, 2336.
[45] G. J. Pahapale, S. Gao, L. H. Romer, D. H. Gracias, *ACS Appl. Bio Mater.* **2019**, *2*, 6004.
[46] M. Zhou, B. H. Lee, Y. J. Tan, L. P. Tan, *Biofabrication* **2019**, *11*, 025011.
[47] L. Ouyang, J. P. Armstrong, Q. Chen, Y. Lin, M. M. Stevens, *Adv. Funct. Mater.* **2019**, *30*, 1908349.
[48] F. R. de Gruijl, H. J. van Kranen, L. H. Mullenders, *J. Photochem. Photobiol. B* **2001**, *63*, 19.
[49] V. Ansteinsson, A. Solhaug, J. T. Samuelsen, J. A. Holme, J. E. Dahl, *Mutat. Res.* **2011**, *723*, 158.
[50] T. Cubaud, T. Mason, *New J. Phys.* **2009**, *11*, 075029.
[51] J. D. Tice, A. D. Lyon, R. F. Ismagilov, *Anal. Chim. Acta* **2004**, *507*, 73.
[52] J. V. Olsen, S.-E. Ong, M. Mann, *Mol. Cell. Proteomics* **2004**, *3*, 608.
[53] M. Cianchetti, C. Laschi, A. Menciassi, P. Dario, *Nat. Rev. Mater.* **2018**, *3*, 143.
[54] S. T. Koshy, R. M. Desai, P. Joly, J. Li, R. K. Bagrodia, S. A. Lewin, N. S. Joshi, D. J. Mooney, *Adv. Healthc. Mater.* **2016**, *5*, 541.
[55] I. A. Babar, C. J. Cheng, C. J. Booth, X. Liang, J. B. Weidhaas, W. M. Saltzman, F. J. Slack, *Proc. Natl. Acad. Sci. USA* **2012**, *109*, E1695.
[56] A. MaHam, Z. Tang, H. Wu, J. Wang, Y. Lin, *Small* **2009**, *5*, 1706.
[57] D. C. Duffy, J. C. McDonald, O. J. Schueller, G. M. Whitesides, *Anal. Chem.* **1998**, *70*, 4974.
[58] A. S. Mao, J.-W. Shin, S. Utech, H. Wang, O. Uzun, W. Li, M. Cooper, Y. Hu, L. Zhang, D. A. Weitz, D. J. Mooney, *Nat. Mater.* **2017**, *16*, 236.